ADVANCED FUNCTIONAL MATERIALS
www.afm-journal.de

Materials Views
www.MaterialsViews.com

Photoinduced Hole Transfer Becomes Suppressed with Diminished Driving Force in Polymer-Fullerene Solar Cells While Electron Transfer Remains Active

Guoqiang Ren, Cody W. Schlenker, Eilaf Ahmed, Selvam Subramaniyan, Selina Olthof, Antoine Kahn, David S. Ginger,* and Samson A. Jenekhe**

Device performance and photoinduced charge transfer are studied in donor/acceptor blends of the oxidation-resistant conjugated polymer poly[(4,8-bis(2-hexyldecyl)oxy)benzo[1,2-b:4,5-b′]dithiophene)-2,6-diyl-alt-(2,5-bis(3-dodecylthiophen-2-yl)benzo[1,2-d;4,5-d′]bisthiazole)] (PBTHDDT) with the following fullerene acceptors: [6,6]-phenyl-C_{71}-butyric acid methyl ester ($PC_{71}BM$); [6,6]-phenyl-C_{61}-butyric acid methyl ester ($PC_{61}BM$); and the indene-C_{60} *bis*-adduct $IC_{60}BA$). Power conversion efficiency improves from 1.52% in $IC_{60}BA$-based solar cells to 3.75% in $PC_{71}BM$-based devices. Photoinduced absorption (PIA) of the PBTHDDT:fullerene blends suggests that exciting the donor polymer leads to long-lived positive polarons on the polymer and negative polarons on the fullerene in all three polymer fullerene blends. Selective excitation of the fullerene in $PC_{71}BM$ or $PC_{61}BM$ blends also generates long-lived polarons. In contrast, no discernible PIA features are observed when selectively exciting the fullerene in a PBTHDDT/$IC_{60}BA$ blend. A relatively small driving force of ca. 70 meV appears to sustain charge separation via photoinduced hole transfer from photoexcited $PC_{61}BM$ to the polymer. The decreased driving force for photoinduced hole transfer in the $IC_{60}BA$ blend effectively turns off hole transfer from $IC_{60}BA$ excitons to the host polymer, even while electron transfer from the polymer to the $IC_{60}BA$ remains active. Suppressed hole transfer from fullerene excitons is a potentially important consideration for materials design and device engineering of organic solar cells.

1. Introduction

Organic semiconductors are finding increasing applications in optoelectronic and electronic devices, such as organic solar cells (OSCs)[1–5] and organic field-effect transistors (OFETs).[6,7] For example, the power conversion efficiency (PCE) of bulk heterojunction (BHJ) solar cells made from organic semiconductors is approaching 10%,[3] demonstrating the potential of organic solar cells as a means of utilizing solar energy.

Oxidation-resistant conjugated polymers, typically those with very negative ionization energies, have attracted increased attention in OFET research, due to their enhanced durability and lengthened operation lifetime in air. For instance, using benzobisthiazole as the electron deficient building block and various other electron rich moieties (dithienosilole, dithienopyrrole, carbazole, and bithiophene), the ionization energy can be tuned by nearly 900 meV, yielding OFETs with remarkably stable (over 2 years in air) hole mobility, threshold voltage, and on/off current ratio.[4i] Further exploring such oxidation-resistant conjugated copolymers for use in organic solar cells with extended operation lifetime is highly desirable. However, making the donor material more difficult to oxidize can complicate device operation as it can decrease the free energy available for driving photoinduced hole transfer from the acceptor material.

Fullerene derivatives have been widely used as the electron acceptors in organic solar cells and have yielded the highest power conversion efficiencies so far.[3] High performance fullerene materials include [6,6]-phenyl-C_{71}-butyric acid methyl ester ($PC_{71}BM$), [6,6]-phenyl-C_{61}-butyric acid methyl ester ($PC_{61}BM$), and indene-C_{60} *bis*-adduct ($IC_{60}BA$). However, chemical modification of fullerenes usually results in modified ionization energy (*IE*) and electron affinity (*EA*) values, as well as changes in film morphology, both of which can affect the photovoltaic properties of solar cells. For example, in $PC_{71}BM$, $PC_{61}BM$ and $IC_{60}BA$, the value of *EA* varies between 3.8 and 4.0 eV.[8]

G. Ren, Dr. E. Ahmed, Dr. S. Subramaniyan, Prof. S. A. Jenekhe
Department of Chemical Engineering
University of Washington
Seattle, WA 98195, USA
E-mail: jenekhe@u.washington.edu
Dr. C. W. Schlenker, Prof. D. S. Ginger
Department of Chemistry
University of Washington
Seattle, WA 98195, USA
E-mail: ginger@chem.washington.edu
Dr. S. Olthof, Prof. A. Kahn
Department of Electrical Engineering
Princeton University
Princeton, NJ 08544, USA
E-mail: kahn@princeton.edu

DOI: 10.1002/adfm.201201470

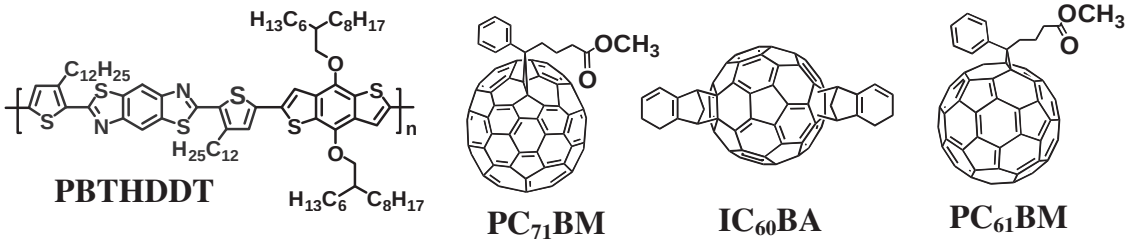

Figure 1. Molecular structures of PBTHDDT donor polymer and three fullerene acceptors ($PC_{71}BM$, $IC_{60}BA$, $PC_{61}BM$) used this study.

In this paper, we study the use of an oxidation-resistant conjugated copolymer, poly[(4,8-bis(2-hexyldecyl)oxy)benzo[1,2-b:4,5-b′]dithiophene)-2,6-diyl-alt-(2,5-bis(3-dodecylthiophen-2-yl)benzo[1,2-d;4,5-d′]bisthiazole)] (PBTHDDT)[4i] in a series of polymer/fullerene blend solar cells. In addition to the technological interest associated with the use of polymers with increased oxidative stability, the use of PBTHDDT is of interest for fundamental studies because the *IE* of the polymer is quite negative relative to vacuum, and is similar to the energy released when transferring an electron to the half-filled highest occupied molecular orbital (HOMO) of the fullerene exciton (the excited state *EA*). We can thus use PBTHDDT/fullerene blends to examine the effects of modulating the driving force for photoinduced hole transfer on the photovoltaic behavior of BHJ polymer solar cells. We find that solar cells based on PBTHDDT:PCBM have much higher power conversion efficiencies (2.70–3.75% PCE) compared with that of ICBA-based devices (1.52% PCE). The photoinduced absorption (PIA) spectra of all the PBTHDDT:fullerene blends exhibit long-lived positive polarons in PBTHDDT and negative polarons on the fullerene when exciting the polymer. However, no induced absorption features are observed when selectively exciting $IC_{60}BA$ blended with PBTHDDT, suggesting that $IC_{60}BA$ excitons do not efficiently generate long-lived charges at the D/A interface. On the other hand, selective excitation of $PC_{71}BM$ or $PC_{61}BM$ blended with PBTHDDT does generate long-lived polarons. We explain these results by using the offset between the ionization energy of the polymer and the electron affinity of the fullerene in its singlet excited state as the measure of the driving force for charge separation via photoinduced hole transfer. Specifically, we find the driving force for photoinduced hole transfer to be insufficient to sustain long-lived charge separation from $IC_{60}BA$ excitons when paired with PBTHDDT.

2. Results and Discussion

2.1. Photovoltaic Properties

We show the molecular structures of poly[(4,8-bis(2-hexyldecyl)oxy)benzo[1,2-b:4,5-b′]dithiophene)-2,6-diyl-alt-(2,5-bis(3-dodecylthiophen-2-yl)benzo[1,2-d;4,5-d′]bisthiazole)] (PBTHDDT) and the three different fullerene derivatives, including $PC_{71}BM$, $PC_{61}BM$, and $IC_{60}BA$, in **Figure 1**. PBTHDDT contains a benzobisthiazole as the electron deficient moiety and a benzodithiophene as the electron rich moiety in the repeating unit.

We first investigated the photovoltaic properties of BHJ solar cells made from PBTHDDT:fullerene blends, where the fullerene acceptor is either $PC_{71}BM$, $PC_{61}BM$, or $IC_{60}BA$. The solar cells have the basic device structure of ITO/PEDOT:PSS/active layer/LiF/Al, where the active layer is a spin-cast film composed of PBTHDDT:fullerene blend with an optimal weight ratio of 1:2, and processed with 2.5 vol% 1,8-diiodooctane (DIO). The solar cells were fabricated in a glovebox and tested under AM1.5 solar illumination at 1 sun (100 mW/cm^2) in ambient air. The current density (*J*)–voltage (*V*) curves for these devices are shown in **Figure 2**a. The photovoltaic parameters of devices made from PBTHDDT:fullerene blends, including the open circuit voltage (V_{oc}), the short-circuit current density (J_{sc}), and fill factors (*FF*) are collected in **Table 1**. V_{oc} increased slightly from 0.64 V in PBTHDDT:$PC_{71}BM$ devices to 0.69 V in PBTHDDT:$PC_{61}BM$ devices, but increased dramatically to 0.95 V in PBTHDDT:$IC_{60}BA$ solar cells. However, we observe a significant reduction in J_{sc} and slight losses in *FF* as well in the $IC_{60}BA$-based solar cells, compared with the $PC_{71}BM$ and $PC_{61}BM$ based devices. For example, a J_{sc} of 3.45 mA/cm^2 in PBTHDDT:$IC_{60}BA$ solar cells represents a 64% and 46% decrease compared to that of PBTHDDT:$PC_{71}BM$ (9.60 mA/cm^2) and PBTHDDT:$PC_{61}BM$ (6.39 mA/cm^2) solar cells, respectively. We observe a small decrease in *FF* to 0.50 for PBTHDDT:$IC_{60}BA$ solar cells (≈20% lower than that of PCBM-based devices). As a result, average power conversion efficiency (PCE) decreased from 3.75 ± 0.06% for PBTHDDT:$PC_{71}BM$, and 2.70 ± 0.05% for PBTHDDT:$PC_{61}BM$, to 1.52 ± 0.07% in PBTHDDT:$IC_{60}BA$ solar cells, with the major efficiency loss due to comparatively low photocurrent generation.

The incident photon-to-electron efficiency (IPCE) or photocurrent action spectrum of each PBTHDDT:fullerene solar cell system is shown in Figure 2b. The photoresponse of PBTHDDT:$PC_{71}BM$ turns on at about 720 nm and peaks at 460–510 nm. The response above 600 nm is due almost entirely to the fullerene, as PBTHDDT has negligible absorbance beyond 600 nm (Supporting Information, Figure S1). The photoresponse of PBTHDDT:$PC_{61}BM$ also begins at ≈720 nm, but is much weaker over the region from ≈720–580 nm due to the reduced absorption in the spherically symmetric fullerene relative to the $PC_{71}BM$. Finally, the PBTHDDT:$IC_{60}BA$ solar cells exhibit the lowest overall photocurrent, and show less than 1% IPCE over the region where only the fullerene absorbs (λ = 600–720 nm). To more clearly illustrate the low photoresponse

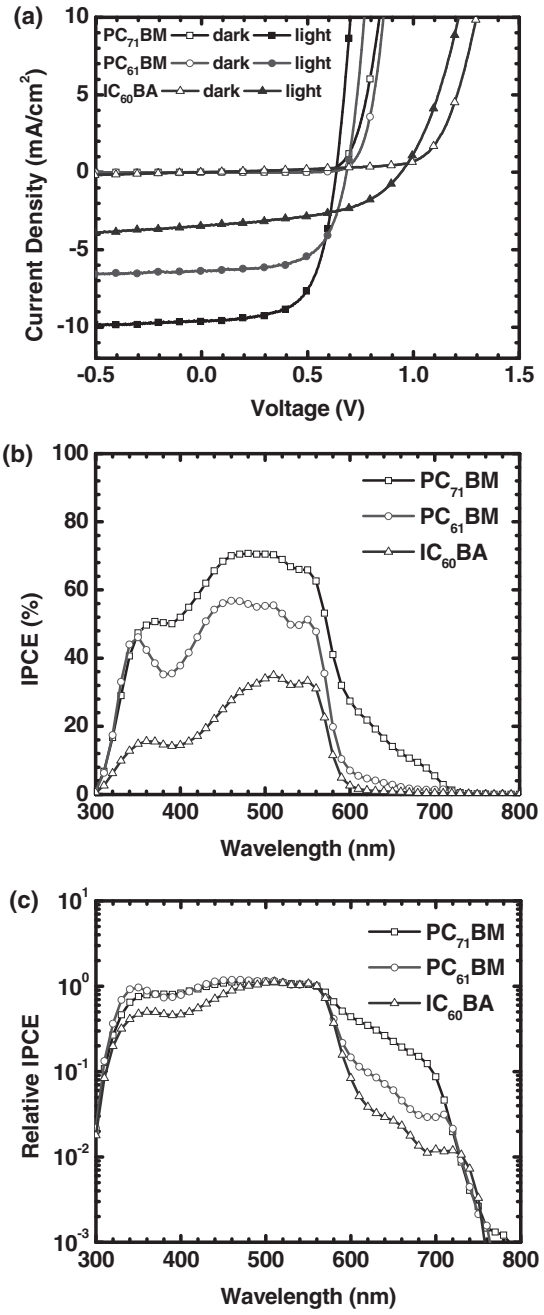

Figure 2. a) Current density (*J*)–voltage (*V*) characteristics, b) IPCE spectra of the PBTHDDT:fullerene (1:2) blend solar cells, and c) semi-logarithmic scale IPCE spectra normalized to PBTHDDT absorption at 560 nm.

from the $IC_{60}BA$ acceptor in this spectral region, Figure 2c shows the IPCE values normalized to the PBTHDDT absorption at ca. 560 nm.

The maximum IPCE was 70% for PBTHDDT:$PC_{71}BM$, 57% for PBTHDDT:$PC_{61}BM$, and 33% for PBTHDDT:$IC_{71}BA$ devices. The expected J_{sc} (calculated from the IPCE spectrum) is 9.00 mA/cm^2 for PBTHDDT:$PC_{71}BM$, 6.13 mA/cm^2 for PBTHDDT:$PC_{61}BM$, and 3.25 mA/cm^2 for PBTHDDT:$IC_{71}BA$. These J_{sc} values calculated from the IPCE spectra are slightly (4.1–6.3%) lower than the J_{sc} obtained in *J*–*V* measurements. This small discrepancy could be due to spectral mismatch between the simulated light source and the AM1.5 solar spectrum or to degradation of the solar cells during measurement since the IPCE data was collected following the *J*–*V* measurement.

For comparison with the PBTHDDT devices, we fabricated BHJ solar cells based on P3HT:fullerene (1:1 w/w) blends, and characterized their photovoltaic performance under similar conditions. We present the *J*–*V* characteristics of our P3HT:fullerene BHJ solar cells in Figure S2 (Supporting Information) and summarize their photovoltaic properties in Table S1 (Supporting Information). Average PCEs of 3.70 ± 0.04%, 3.15 ± 0.05%, and 4.32 ± 0.09% were achieved in P3HT:$PC_{71}BM$, P3HT:$PC_{61}BM$, and P3HT:$IC_{60}BA$ solar cells, respectively. The increasing trend in PCE as $PC_{61}BM$, $PC_{71}BM$, and $IC_{60}BA$ are used as the electron acceptor in BHJ solar cells agrees well with previous observations.[4f,k] Briefly, the enhancement in PCE in P3HT:$PC_{71}BM$ compared to that of P3HT:$PC_{61}BM$ is primarily due to the enhanced absorption in the visible region and optimized nanoscale morphology in P3HT:$PC_{71}BM$ films.[9] P3HT:$IC_{60}BA$ solar cells have a higher V_{oc} (0.79 V) than that of P3HT:PCBM devices (0.61 V), while the other photovoltaic parameters (J_{sc} and *FF*) are similar to those of P3HT:PCBM devices, resulting in higher overall power conversion efficiency.[4f,8b]

We further compared the photovoltaic properties of BHJ solar cells based on the same fullerene acceptor. PBTHDDT:$PC_{71}BM$ and P3HT:$PC_{71}BM$ solar cells showed similar photovoltaic parameters (V_{oc}, J_{sc}, and *FF*), and similar photovoltaic efficiency (3.75% vs 3.70%). Using $PC_{61}BM$ as the acceptor in BHJ solar cells, we observe a 14% decrease in PCE for PBTHDDT:$PC_{61}BM$ devices, compared with that of P3HT:$PC_{61}BM$ solar cells, with the slight decrease in PCE being largely attributable to a comparable decrease in the J_{sc} due to the slightly bluer absorption onset of PBTHDDT relative to P3HT. The observed increase in V_{oc} in PBTHDDT:$IC_{60}BA$ devices is understandable considering the increased diagonal energy offset $\Delta E_{DA} = IE$[Donor]–*EA*[Acceptor] of that blend.[10] The decrease of J_{sc} and *FF* in PBTHDDT:$IC_{60}BA$ solar cells, compared with those of P3HT:$IC_{60}BA$ solar cells, is critical in explaining the observed difference in photovoltaic properties. We therefore focused a detailed study on the morphology, optical and photophysical properties of PBTHDDT:fullerene blend films to look for the reason for the reduction in J_{sc} and *FF* when ICBA is used as the electron acceptor instead of PCBM.

2.3. Morphology

Figure 3 shows bright-field transmission electron microscope (BF-TEM) images of the nanomorphology of PBTHDDT:fullerene blend films (≈80 nm thick) directly peeled off from the solar cells. The images were taken at a slightly defocused condition to enhance the phase contrast between polymer and fullerene, with fullerene-rich domains often appearing darker under BF-TEM due to their higher density than the polymer-rich domains.[11] The TEM images of PBTHDDT:$PC_{61}BM$ and PBTHDDT:$IC_{60}BA$

Table 1. Device metrics and energies offsets of PBTHDDT:fullerene blend solar cells. Energy differences are calculated in eV from the average of film CV, solution, CV, and PES data.

Blend[a)]	V_{oc} [V]	J_{sc} [mA/cm^2]	*FF*	η_{max} [% PCE]	η_{ave} [% PCE]	ΔE_{Hole}[b)]	ΔE_{Elec}[b)]	ΔE_{DA}[c)]
PBTHDDT:$PC_{71}BM$	0.64	9.60	0.63	3.83	3.75 ± 0.06	–0.133	–0.403	–1.68
PBTHDDT:$PC_{61}BM$	0.69	6.39	0.62	2.72	2.70 ± 0.05	–0.066	–0.376	–1.70
PBTHDDT:$IC_{60}BA$	0.95	3.45	0.50	1.62	1.52 ± 0.07	0.110	–0.250	–1.83

[a)]1:2 wt:wt blend ratio; [b)]See Equation 2; [c)]$\Delta E_{DA} = IE$[Donor]–EA[Acceptor].

blends showed similar nanomorphology (Figure 3c,d), containing long fibrillar nanostructures. A low density of bright features were observed in the PBTHDDT:$IC_{60}BA$ blend films (Figure 3e,f), possibly suggesting the presence of larger aggregates in this blend. Similar aggregates were not observed in either P3HT:$IC_{60}BA$ (Supporting Information Figure S3e,f) or PBTHDDT:PCBM (Figure 3a–d) blend films. Overall, however we observe similar morphology by TEM imaging among all three of our PBTHDDT:fullerene blends. We also used atomic force microscopy (AFM) to characterize the surface topography of the active layer on the actual solar cells. We present topographical AFM images for a 5 μm × 5 μm region of each PBTHDDT:fullerene blend film in **Figure 4**. All the blend films showed similar surface topography with surface features less than 50 nm in height. The root-mean-square roughness (R_q) among these blend films was comparable, with values as follows: PBTHDDT:$PC_{71}BM$ (3.89 nm), PBTHDDT:$PC_{61}BM$ (4.05 nm), and PBTHDDT:$IC_{60}BA$ (3.54 nm). From these data we are unable to identify an obvious large-scale source of morphological variation that could explain the large efficiency differences between the different PBTHDDT/fullerene blends. Therefore, as we discuss in the following sections, we turned to optical spectroscopy to examine the photophysical and energetic differences between the films.

2.4. Photophysical Properties of Polymer:Fullerene Blends

Figure 5 compares the absorption spectra of PBTHDDT:$PC_{71}BM$, PBTHDDT:$PC_{61}BM$, and PBTHDDT:$IC_{60}BA$ blend films. The optical densities near 450 nm for the PBTHDDT:$IC_{60}BA$ and PBTHDDT:$PC_{61}BM$ blends are comparable (ca. OD = 0.24). As expected, they are both lower than that of PBTHDDT:$PC_{71}BM$ blends (ca. OD = 0.35). The difference in optical density between the $PC_{71}BM$ blend and the $PC_{61}BM$ or $IC_{60}BA$ blends is due to the enhanced absorbance of $PC_{71}BM$ in the visible region of the spectrum (Supporting Information Figure S1). However, despite the similar optical density in PBTHDDT:$PC_{61}BM$ and

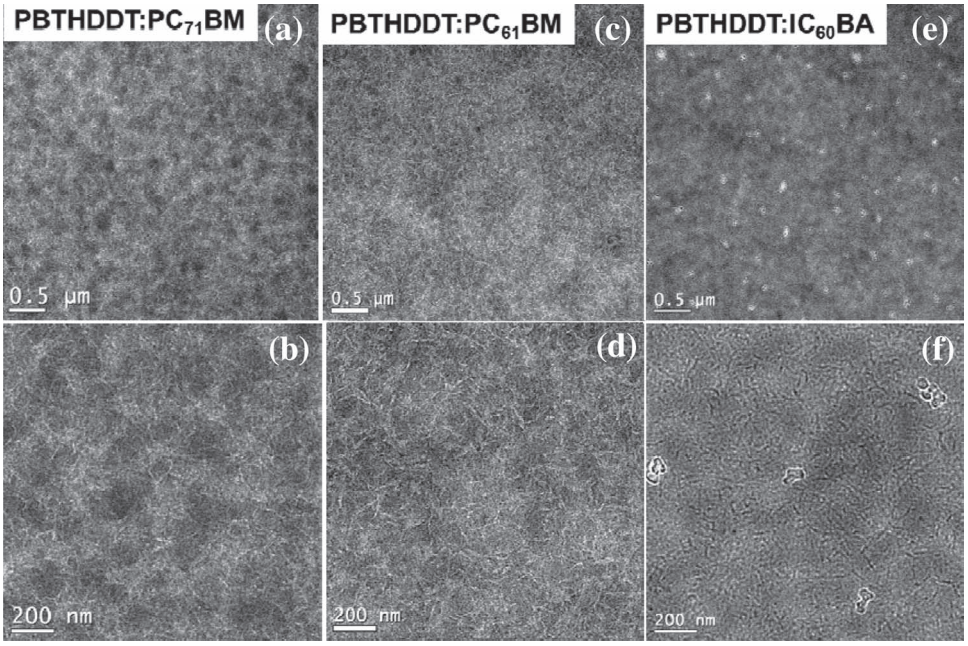

Figure 3. TEM images of PBTHDDT:fullerene (1:2) blend films. a,b) PBTHDDT:$PC_{71}BM$, c,d) PBTHDDT:$PC_{61}BM$, and e,f) PBTHDDT:$IC_{60}BA$.

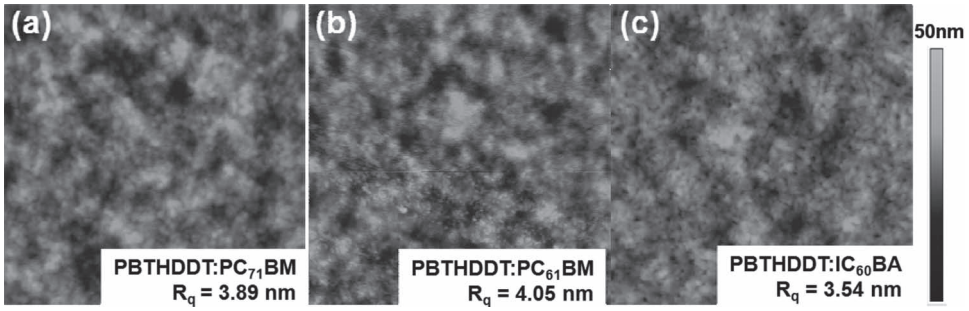

Figure 4. AFM topographical images (5 μm × 5 μm) of PBTHDDT:fullerene blend solar cells.

PBTHDDT:$IC_{60}BA$ blend solar cells, the measured IPCE for the $IC_{60}BA$ device in this spectral region is 75% lower than that of the $PC_{61}BM$ device.

We employed spectroelectrochemical measurements and photoinduced absorption (PIA) spectroscopy to understand the different photocurrent responses in our PBTHDDT:$IC_{60}BA$ solar cells. Polaron optical signatures arising from photoinduced radicals are commonly observable in the PIA spectra for polymer:fullerene blends.[12] To identify the expected spectral signature for $PBTHDDT^+$ radical cation (polaron spectrum) **Figure 6**a shows a differential absorption ($\Delta OD = OD_{Oxidized} - OD_{Neutral}$) spectrum for an electrochemically-oxidized neat film of PBTHDDT on ITO (open circle trace in Figure 6a). The ΔOD spectrum exhibits a distinct oxidatively induced absorption feature corresponding to absorption by the polymer cation at λ = 790 nm labeled $PBTHDDT^+$.

The PIA experiment is a pump-probe technique that measures the optical absorption of long-lived excited states (e.g., polarons or triplets with lifetime, τ, on the order of microseconds to milliseconds) resulting from excitation by a frequency modulated monochromatic excitation source. We plot the normalized differential transmittance data ($\Delta T/T$) in terms of the differential thin film absorption coefficient as $\Delta\alpha d = -\ln[1 + \Delta T/T]$. The solid black trace in Figure 6a representing the PIA spectrum (right y-axis) for a neat film of PBTHDDT (excitation at λ = 455 nm), exhibits a significantly different spectral fingerprint than the oxidized form of the polymer collected by spectroelectrochemical methods, suggesting that few if any polarons are formed upon photoexcitation

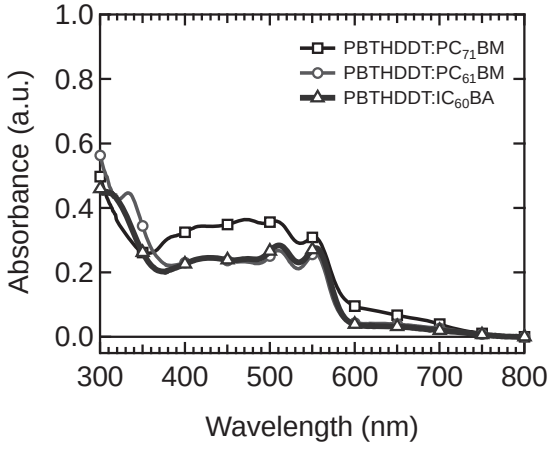

Figure 5. UV-vis absorption spectra of PBTHDDT:fullerene blend films.

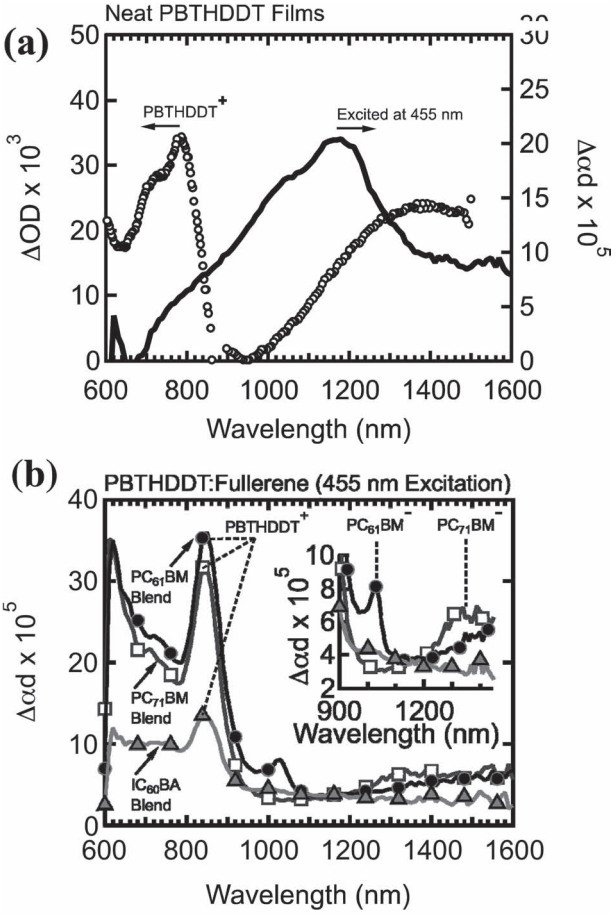

Figure 6. a) Spectroelectrochemical differential absorption (open circles) of a PBTHDDT film ($\Delta OD = OD_{Oxidized} - OD_{Neutral}$) showing an electrochemically induced $PBTHDDT^+$ polaron absorption peak at λ = 790 nm. The photoinduced absorption (PIA) spectrum (solid line, excited at 455 nm) on the right ordinate ($\Delta\alpha d = -\ln[1 + \Delta T/T]$) for a pristine film of PBTHDDT exhibits a peak at λ = 1170 nm consistent with polymer triplet absorption. ΔOD measured in transmission mode on ITO in CH_3CN:$(C_4H_9)_4N(ClO_4)$. b) PIA spectra for PBTHDDT:fullerene blends ($PC_{61}BM$ blend = filled circles, $PC_{71}BM$ blend = open squares, and $IC_{60}BA$ blend = filled triangles) when both components are excited at 455 nm. Peaks consistent with PBTHDDT polarons at λ = 850 nm are labeled $PBTHDDT^+$. Inset depicts the spectral region for λ > 900 nm, where peaks consistent with fullerene anion generation are observed at λ = 1030 nm ($PC_{61}BM^-$, filled circles) and λ = 1340 nm ($PC_{71}BM^-$, open squares). The weak feature at λ = 1010 nm (filled triangles) is consistent with $IC_{60}BA^-$ generation. All $\Delta\alpha d$ recorded at 80 K under 455 nm excitation modulated at 200 Hz.

of the neat film. At 80 K, the neat film exhibits a broad PIA feature that peaks at ca. $\lambda = 1180$ nm. The intensity of this NIR feature increases by two orders of magnitude upon cooling from room temperature to $T = 80$ K and exhibits non-dispersive decay with increasing modulation frequency. Based on the temperature dependence, frequency dependence, and the absence of any such feature in the spectroelectrochemical data in Figure 6a we assign this PIA signal at $\lambda = 1180$ nm to $T_1 - T_n$ absorption by PBTHDDT triplet excitons, probably generated via intersystem crossing from the S_1 singlet state excited by 455 nm light.

The PIA spectra for PBTHDDT:fullerene blends under 455 nm excitation are presented in Figure 6b. Note that the polymer and each of the fullerenes absorb 455 nm light. Thus, the resulting PIA features arise from processes involving excitons created on either the donor or the acceptor. Between the wavelength range $\lambda = 700$ nm and 900 nm the PIA signals for each blend are qualitatively similar, exhibiting sharp induced absorption features peaking at $\lambda = 850$ nm (slightly red shifted from the PBTHDDT$^+$ peak we observe by spectroelectrochemistry). Given the resemblance of the PIA signals observed in this spectral region to that obtained for the electrochemically oxidized polymer in Figure 6a, we assign this feature to a positive PBTHDDT$^+$ polaron on the polymer backbone. Fullerene anion peaks are also apparent in the PIA spectra for $PC_{71}BM$ (1340 nm)[13] and $PC_{61}BM$ (1030 nm)[14] (see inset Figure 6b). In the $IC_{60}BA$-based blend an extremely weak feature near 1010 nm may also suggest the presence of fullerene anion resulting when the sample is illuminated with 455 nm excitation. We note that no discernible polymer triplet features appear at 1180 nm in any of the blends examined in Figure 6b, suggesting that polymer excitons are quenched prior to intersystem crossing and charge recombination to the polymer triplet state is negligible.

Although the optical densities (Figure 5) are nearly equivalent at the excitation wavelength ($\lambda = 455$ nm) for the PBTHDDT:$IC_{60}BA$ blend and the PBTHDDT:$PC_{61}BM$ blend, the PIA signature corresponding to PBTHDDT$^+$ polarons in the $IC_{60}BA$ blend ($\Delta\alpha d = 1.3 \times 10^{-4}$) is more than a factor of 2.5 lower than that observed for the analogous fullerene methyl ester blend (PBTHDDT:$PC_{61}BM$, $\Delta\alpha d = 3.6 \times 10^{-4}$). This result suggests fewer long lived charges are being formed per absorbed photon, and is in qualitative agreement with the lower photocurrent density and IPCE measured for the corresponding $IC_{60}BA$ devices.

Upon direct excitation of the fullerene, the PBTHDDT:$IC_{60}BA$ blends produce less photocurrent than the PBTHDDT:$PC_{61}BM$ blend (Figure 2c), despite the fact that the two different active layers show nearly equal absorption amplitude at 630 nm (Figure 5). Based on this observation we hypothesized that photoinduced hole transfer from $IC_{60}BA$ singlet excitons to PBTHDDT may not be occurring, which would indicate that charge generation in the PBTHDDT:$IC_{60}BA$ may primarily involve polymer exciton dissociation, with minimal harvesting of fullerene excitons.

To test this hypothesis, we compared the PIA signal measured for PBTHDDT:$IC_{60}BA$ to that measured for PBTHDDT:$PC_{61}BM$ while selectively exciting the fullerene component at 630 nm. The PBTHDDT polymer is completely transparent at this wavelength; therefore, PIA signals in the blend measured under 630 nm excitation originate uniquely from photoexcitation of the fullerene. **Figure 7**a shows the resulting PIA data, with the

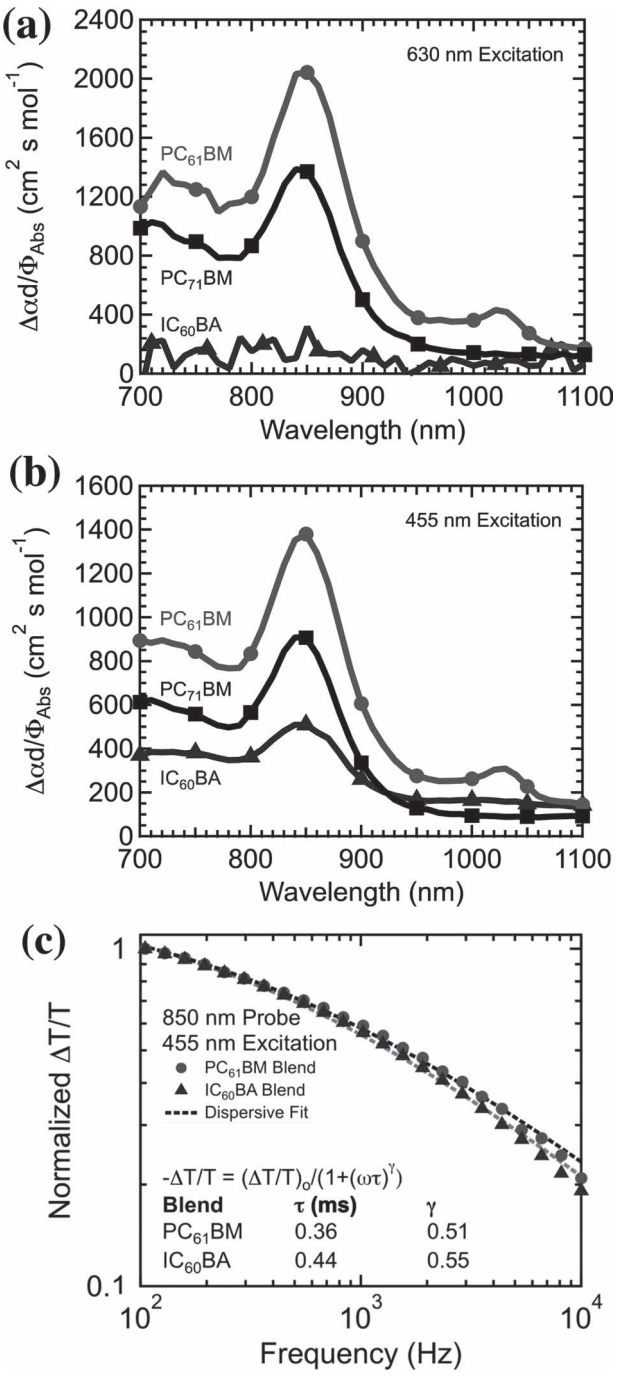

Figure 7. a) Photoinduced absorption ($\Delta\alpha d$) spectra scaled by the photon flux absorbed (Φ_{Abs}) by selectively exciting the fullerene at 630 nm in PBTHDDT:fullerene blends ($PC_{61}BM$ blend = circles, $IC_{60}BA$ blend = triangles, $PC_{71}BM$ = squares). b) $\Delta\alpha d/\Phi_{Abs}$ spectra collected when both blend components are simultaneously excited at 455 nm for each PBTHDDT:fullerne blend using the same symbols as in a). c) Modulation frequency dependence of the differential transmittance ($-\Delta T/T \approx \Delta\alpha d$) monitored at 850 nm (PBTHDDT$^+$ polaron peak) for the $PC_{61}BM$ (circles) and $IC_{60}BA$ (triangles) blends in a) under 455 nm excitation. Decay parameters (τ) according to the inset model were obtained from dispersive fits (dashed lines) to the data as a function of modulation frequency $f = \omega/(2\pi)$. All PIA data were collected at 80 K.

signal magnitudes scaled by the absorbed photon flux at the excitation wavelength (Φ_{Abs} with unit of mol cm^{-2} s^{-1}). Importantly, selectively exciting $PC_{61}BM$ in the polymer blend leads to a significant population of PBTHDDT$^+$ polarons ($\Delta\alpha d/\Phi_{Abs} \approx$ 2000 cm^2 s mol^{-1} at 850 nm) in the PIA spectrum, indicating that $PC_{61}BM$ excitons reaching the PBTHDDT interface can undergo efficient charge transfer quenching. However, when we selectively excite the fullerene in the PBTHDDT:$IC_{60}BA$ blend at 630 nm (triangles in Figure 7a) we observe no discernible induced absorption features. For comparison, we have plotted $\Delta\alpha d/\Phi_{Abs}$ in Figure 7b for the PBTHDDT:$PC_{61}BM$ blend collected using 455 nm (circles) and note that the PBTHDDT$^+$ polaron signal magnitude obtained from selectively exciting $PC_{61}BM$ is comparable to that obtained from concomitant excitation of both blend components. Assuming a similar peak intensity ratio for excitation of the fullerene in the PBTHDDT:$IC_{60}BA$ blend, we would expect to observe a PBTHDDT$^+$ PIA feature with signal magnitude $\Delta\alpha d/\Phi_{Abs} \approx$ 720 cm^2 s mol^{-1} appearing at 850 nm when the $IC_{60}BA$ in the blend is excited with 630 nm light. However, we observe instead an extremely weak and poorly resolved feature in Figure 7a (triangles) at 850 nm ($\Delta\alpha d/\Phi_{Abs} \approx$ 315 cm^2 s mol^{-1}) approaching the noise floor of our instrumentation ($\Delta\alpha d/\Phi_{Abs} \approx$ 100 cm^2 s mol^{-1}). We may take this as an upper limit for the relative dissociation efficiency of $IC_{60}BA$ excitons compared to $PC_{61}BM$ excitons at the PBTHDDT interface, suggesting that the photoinduced hole transfer efficiency of $IC_{60}BA$ excitons is less than 20% that of $PC_{61}BM$ excitons.

Finally, we plot the dependence of the normalized PBTHDDT$^+$ PIA signal intensity as a function of modulation frequency in Figure 7c for PBTHDDT:$IC_{60}BA$ (triangles) and PBTHDDT:$PC_{61}BM$ (circles). The two traces exhibit nearly identical characteristic roll-off behavior that may be fit using the simple dispersive decay model[15] presented in the inset of Figure 7c, with nearly equivalent lifetime fitting parameters of $\tau \approx 0.40$ ms in both blends.[16] Thus, the significantly lower PBTHDDT$^+$ signal obtained when exciting the PBTHDDT:$IC_{60}BA$ blend at 455 nm in Figure 7a cannot be attributed to faster recombination in the PBTHDDT:$IC_{60}BA$ compared to the PBTHDDT:$PC_{61}BM$ blend.

These data suggest that a portion of the polymer excitons in all of the polymer:fullerene blends examined here leads to long-lived positive polarons on the polymer and negative polarons on the fullerene. While $PC_{71}BM$ and $PC_{61}BM$ excitons appear to undergo hole transfer at the D/A interface, generating long-lived charges in the PBTHDDT:PCBM blends, excitons on the $IC_{60}BA$ do not appear to efficiently produce long-lived charges at the D/A interface. We next examine this result in the context of the expected driving forces for photoinduced charge separation via electron and hole transfer in these blends.

2.5. Driving Force for Photoinduced Charge Transfer

To identify qualitative trends in the energy landscape resulting from PBTHDDT with different fullerene acceptors we compare energies tabulated from cyclic voltammetry (CV for thin film and solution samples measured in this work and compared against solution values taken from literature)[8b,17] with those derived from photoemission spectroscopy (PES).

Importantly, rather than using the common approximation of frontier orbital energies[18] to estimate the driving force for photoinduced charge separation we instead follow the established electrochemical convention[19] of calculating the exited state oxidation potential (the potential required to oxidize the material in its excited state) of the donor and the excited state reduction potential (the potential required to reduce the material in its excited state) of the acceptor. We extend this convention to the solid state *IE*, and the *EA* of ground state materials compared to those in the excited state as previously proposed.[20] Using the value of the singlet exciton energy E_g^{Opt} we estimate the electron affinity of the excited state ($EA_{(M^*/M^-)}$) as given by Equation 1a. Similarly, we calculate the excited state ionization energy ($IE_{(M^+/M^*)}$) of the donor according to Equation 1b. We note that this convention is similar to the effective HOMO and effective lowest unocupied molecular orbital (LUMO) convention used by Veldmann et al.[21] in that it accounts for the binding energy of the exciton. However, our convention differs with regard to the driving force for generating separated charges being defined as the energy associated with a particular exciton undergoing dissociation with a ground-state charge acceptor rather than splitting the exciton binding energy between the HOMO and LUMO of each material and adding the coulomb energy to calculate the energy of the bound charge transfer state.

$$EA_{(M^*/M^-)} = EA_{(M/M^-)} - E_g^{Opt} \quad (1a)$$

$$IE_{(M^+/M^*)} = IE_{(M^+/M)} + E_g^{Opt} \quad (1b)$$

Following this convention, in **Scheme 1** we illustrate that an acceptor material under illumination with energy $h\nu \geq E_g^{Opt}$ will engage in spontaneous charge separation via hole transfer to the donor if the value of $EA_{(M^*/M^-)}$ for the acceptor is more negative than the value of *IE* for the donor material. We assume the energy difference ΔE_{Hole} calculated from Equation 2a to satisfactorily approximate the change in free energy (ΔG)[22] for charge separation via photoinduced hole transfer. A similar analysis can be applied using Equation 2b to calculate ΔE_{Elec} to assess whether a given donor exciton is likely to undergo charge separation via electron transfer to a given acceptor:

$$\Delta E_{Hole} = EA_{(M^*/M^-)}\,[\text{Acceptor}] - IE_{(M^+/M)}\,[\text{Donor}] \quad (2a)$$

$$\Delta E_{Elec} = EA_{(M/M^-)}\,[\text{Acceptor}] - IE_{(M^+/M^*)}\,[\text{Donor}] \quad (2b)$$

Using this convention, in **Figure 8** we plot the estimated energies related to the driving forces for photoinduced charge separation in our different PBTHDDT/fullerene blends. The CV oxidation/reduction waves, ultraviolet photoemission spectroscopy (UPS), and inverse photoemission spectroscopy (IPES) traces used to estimate energies relative to vacuum in Figure 8 are presented in Figure S4 and S5, respectively, in the Supporting Information. As previously observed[4i] PBTHDDT exhibits an irreversible oxidation wave in thin film as well as solution, thus we must regard the *IE* plotted in Figure 8 based on the CV data as a lower limit, with the true value possibly

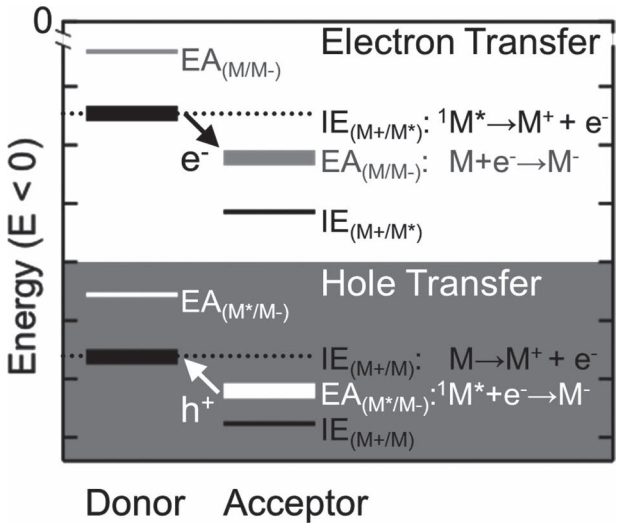

Scheme 1. The driving force for charge separation proceeding through photoinduced hole transfer indicated by the large white arrow labeled h^+ from the acceptor to the donor is related to the difference in the excited state electron affinity ($EA_{(M^*/M^-)}$ = white lines) of the acceptor exciton (heavy-weight white line) and the ground state ionization energy ($IE_{(M+/M)}$ = black lines in the lower "hole transfer" panel) of the donor (heavy-weight black line in the lower panel). Charge separation via hole transfer will occur spontaneously in donor/acceptor pairs for which $IE_{(M+/M)}$[Donor] is more positive than $EA_{(M^*/M^-)}$[Acceptor]. The analogous electron transfer process indicated by the large black arrow labeled e^- will be spontaneous when the excited state ionization energy ($IE_{(M+/M^*)}$ = black lines in upper "electron transfer" panel) of the donor (heavy-weight black line) is more positive than the ground state electron affinity ($EA_{(M/M^-)}$ = dark grey lines) of the acceptor (heavy-weight dark grey line). Light-weight solid lines follow the same shading scheme, with the black light-weight lines in the upper and lower panels depicting $IE_{(M+/M^*)}$ and $IE_{(M+/M)}$, respectively. The grey light-weight lines in the upper and lower panels depict $EA_{(M/M^-)}$ and $EA_{(M^*/M^-)}$, respectively.

being slightly more positive. Photoelectron spectroscopy measurements yielded a featureless spectrum for PBTHDDT where the density of states showed an exponential decay into the band gap. Therefore, an onset of the density of states is very hard to place. The reason for this lies most likely in the long hydrocarbon side chains attached to the polymer that commonly dominate the photoemission spectra and tend to shield the *IE* and *EA* features. Given the potential inaccuracies in estimating absolute *IE* values for PBTHDDT using a single method, we present self-consistent estimates for each material using three methods (film CV, solution CV and film PES) in Figure 8, arriving at qualitatively equivalent conclusions based on each method. We calculated the energy changes relevant for charge separation (ΔE_{Hole} and ΔE_{Elec} calculated from Equation 2 and tabulated in Table 1) in PBTHDDT solar cells from the *IE* and *EA* values in **Tables 2** and **3**.

From the values plotted in Figure 8 we conclude that charge separation by forward electron transfer from photoexcited PBTHDDT to each of the fullerenes should be spontaneous, ($IE_{(M+/M^*)}$[Donor] > $EA_{(M/M^-)}$[Acceptor] giving $\Delta E_{Elec} < 0$ based on Equation 2b). On the other hand, we anticipate spontaneous hole transfer from photoexcited $PC_{71}BM$ to PBTHDDT ($IE_{(M+/M)}$[Donor] > $EA_{(M^*/M^-)}$[Acceptor] giving $\Delta E_{Hole} < 0$), but not from $IC_{60}BA$ to PBTHDDT ($IE_{(M+/M)}$[Donor] < $EA_{(M^*/M^-)}$[Acceptor] giving $\Delta E_{Hole} > 0$). Since the value of $IE_{(M+/M)}$[Donor] is nearly equal to $EA_{(M^*/M^-)}$[Acceptor] for $PC_{61}BM$ paired with PBTHDDT, the energy difference for hole transfer among each method is negative, with an average value of only ΔE_{Hole} = –0.070 eV, suggesting that, while photoinduced hole transfer will be spontaneous, the driving force is relatively small. We arrive at qualitatively identical conclusions based on the solution electrochemical data for PBTHDDT (Supporting Information Figure S4) compared against the solution reduction potentials of $PC_{71}BM$, $PC_{61}BM$, and $IC_{60}BA$ previously reported literature values.[8a]

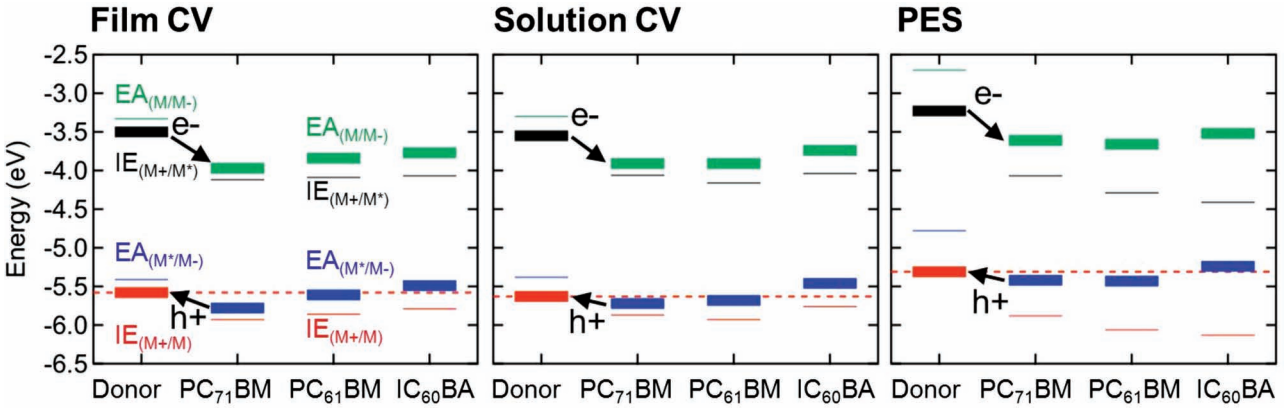

Figure 8. Excited state electron affinity values ($EA_{(M^*/M^-)}$ = heavy-weight blue lines) relevant for estimating whether photoinduced hole transfer (h^+) from each fullerene exciton to the "donor" polymer PBTHDDT (ground state ionization energy *IE* = heavy-weight red lines) will occur spontaneously (*IE*[Donor] more positive than $EA_{(M^*/M^-)}$[Acceptor]). The analogous electron transfer process (e^-) will be spontaneous when the excited state ionization energy ($IE_{(M+/M^*)}$ = black lines and defined numerically in the text) of the donor is more positive than the ground state electron affinity (*EA* = green lines) of the acceptor. "Film CV" denotes energies tabulated from thin film cyclic voltammetry, "Solution CV" denotes energies tabulated from solution cyclic voltammetry with $PC_{71}BM$ from ref. [17a] and $PC_{61}BM$, $IC_{60}BA$ from ref. [8b], and "PES" denotes energies tabulated from ultraviolet photoemission spectroscopy (UPS) and inversion photoemission spectroscopy (IPES). Light-weight black and red lines depict $IE_{(M+/M^*)}$ and $IE_{(M+/M)}$, respectively. Green and blue light-weight lines depict $EA_{(M/M^-)}$ and $EA_{(M^*/M^-)}$, respectively.

Table 2. Energies relevant to charge separation via hole transfer.

Material	$IE_{(M^+/M)}$ from Film CV	$EA_{(M^*/M^-)}$ from Film CV[b)]	$IE_{(M^+/M)}$ from Solution CV	$EA_{(M^*/M^-)}$ from Solution CV[a,b)]	$IE_{(M^+/M)}$ from PES	$EA_{(M^*/M^-)}$ from PES[b)]
PBTHDDT	–5.58	–	–5.63	–	–5.31	–
$PC_{71}BM$	–	–5.78	–	–5.72	–	–5.42
$PC_{61}BM$	–	–5.61	–	–5.68	–	–5.43
$IC_{60}BA$	–	–5.49	–	–5.46	–	–5.24

[a)]Energies in eV tabulated based on ref. [17a]; [b)]Excited state EA calculated based on Equation 1a.

Importantly, the CV and PES data can account for the experimental device and PIA data (dramatically reduced photocurrent and PIA signal when selectively exciting $IC_{60}BA$) only when the state conventions are used. As seen from the positions of the thin lines in Figure 8, a simple analysis based on the position of the ground state *EA*/*IE* values (or HOMO/LUMO levels as is sometimes casually referred to in the OPV literature), suggests that each of the fullerene blends examined here should form a staggered type-II heterojunction with PBTHDDT and thus should support both excited-polymer-to-fullerene electron transfer, and excited-fullerene-to-polymer hole transfer. In contrast, use of the excited state *EA*/*IE* values also predicts that the photoexcited polymer should transfer an electron to all three fullerenes, but correctly predicts that only the photoexcited $PC_{61}BM$ and $PC_{71}BM$ (but not $IC_{60}BA$) should transfer a photoexcited hole back to the polymer.

While we have focused on the primary loss in EQE above, there is also a difference in *FF* between the $PC_{61}BM$ and $IC_{60}BA$ blends. There are several possible origins for this *FF* difference in the context of our findings. First, the value of $EA_{(M^*/M-)}$ for $IC_{60}BA$ is slightly more positive than that of $IE_{(M^+/M)}$ for PBTHDDT, suggesting that photogenerated charges in the $IC_{60}BA$ blend might have an additional thermodynamically plausible pathway for charge recombination (i.e. free charges may recombine to form $IC_{60}BA$ singlet excitons). Free charges engaging in this additional recombination process would lead to diminished FF for PBTHDDT:$IC_{60}BA$ devices compared with PCBM devices. However, attempts to test this hypothesis via photoluminescence have been inconclusive, since we observe overlapping fluorescence from both blend components in all three PBTHDDT blends that we have examined. Moreover, as discussed above, in both $PC_{61}BM$ and $IC_{60}BA$ blends we observe a nearly identical polaron lifetime (based on the modulation frequency dependence in our photoinduced absorption measurements). These results could thus also be consistent with the result of differences in field dependent charge carrier separation/geminate recombination rates arising from the lower driving force for electron transfer from the polymer to $IC_{60}BA$ compared to $PC_{61}BM$.

Finally, we note that Förster resonant excitation transfer (FRET) from the donor polymer to the fullerene has been observed for many polymer:fullerene systems,[23] when the singlet excited state of the donor is higher in energy than that of the acceptor. Since the S_1 energy of the PBTHDDT is roughly 360 meV above that of $IC_{60}BA$, it is likely that the FRET process from PBTHDDT to $IC_{60}BA$ competes with exciton dissociation from the polymer. Although we cannot observe distinct transient species indicative of this FRET process in our quasi-steady state photoinduced absorption measurement, we believe it is likely that the origin of the poor overall polaron generation and low photocurrent in these $IC_{60}BA$ devices arises from singlet excitation transfer from the polymer to the fullerene and extremely poor fullerene exciton dissociation. This is reflected in the IPCE of PBTHDDT:$IC_{60}BA$ being 53% lower and the PIA signal being 63% lower than the PBTHDDT:$PC_{61}BM$ when both the polymer and the fullerene are excited at 455 nm, despite the two blends exhibiting identical decays with increasing modulation frequency.

3. Conclusions

We have investigated the impact that modulating the driving force for photoinduced hole transfer has on the photovoltaic

Table 3. Energies relevant to charge separation via electron transfer.

Material	$IE_{(M^+/M^*)}$ from Film CV[b)]	$EA_{(M/M^-)}$ from Film CV	$IE_{(M^+/M^*)}$ from Solution CV[b)]	$EA_{(M/M^-)}$ from Solution CV[a)]	$IE_{(M^+/M^*)}$ from PES[b)]	$EA_{(M/M^-)}$ from PES
PBTHDDT	–3.50	–	–3.55	–	–3.23	–
$PC_{71}BM$	–	–3.97	–	–3.91	–	–3.61
$PC_{61}BM$	–	–3.84	–	–3.91	–	–3.66
$IC_{60}BA$	–	–3.77	–	–3.74	–	–3.52

[a)]Energies in eV tabulated based on ref. [8b] and [17a]; [b)]Excited state IE calculated based on Equation 1b.

properties of bulk heterojunction solar cells using an oxidation-resistant copolymer semiconductor, PBTHDDT, and various fullerene derivatives. We found that solar cells based on PBTHDDT:$PC_{71}BM$, PBTHDDT:$PC_{61}BM$ and PBTHDDT:$IC_{60}BA$ blends showed average efficiency of 3.75%, 2.70%, and 1.52% PCE, respectively. At a coarse level we observe similar nanoscale features among the different PBTHDDT:fullerene blends by TEM and AFM imaging. While these data do not address molecular level packing and orientation effects, they suggest that large-scale morphological changes are unlikely to be the source of the significant observed variation in photovoltaic performance. Photophysical studies of the PBTHDDT:fullerene blends showed that all the PBTHDDT:fullerene blends generated long-lived positive polarons in PBTHDDT and negative polarons on the fullerene upon photoexcitation of the polymer. While fullerene excitons in PBTHDDT:$PC_{71}BM$ and PBTHDDT:$PC_{61}BM$ blends appear to undergo photoinduced hole transfer at the donor/acceptor interface to generate long-lived polarons, selective excitation of the fullerene in PBTHDDT:$IC_{60}BA$ blends does not efficiently produce long-lived charges. Thus, at least part of the low photocurrent observed in the PBTHDDT:$IC_{60}BA$ blend solar cells is attributable to the low quantum yield for charge generation/separation of $IC_{60}BA$ excitons. We attribute this low dissociation efficiency to the small driving force for hole transfer at the polymer/$IC_{60}BA$ interface being insufficient to sustain efficient charge separation. Comparing these results with the CV and PES data, we find they are consistent in a state energy level picture but not a simplified frontier orbital picture. While our analysis is based purely on thermodynamic parameters, we point out that kinetic factors can also play an important role in determining overall charge separation efficiency in some systems, as previous authors have suggested.[22,24]

Although the fullerene itself is not responsible for the bulk of the light absorption in this blend, energy transfer from the polymer to the fullerene has been proposed in many systems,[25] and poor fullerene exciton dissociation could thus represent a significant loss mechanism. Neglecting undetected morphological changes, our results would suggest that the efficiency of fullerene exciton dissociation at the polymer/fullerene interface drops by ≈80% when $PC_{61}BM$ is replaced with $IC_{60}BA$ in PBTHDDT:fullerene blends. These results provide an important guide for materials design and device engineering in bulk heterojunction polymer solar cells.

4. Experimental Section

Materials: The synthesis and characterization of poly[(4,8-bis(2-hexyldecyl)oxy)benzo[1,2-b:4,5-b′]dithiophene)-2,6-diyl-alt-(2,5-bis(3-dodecylthiophen-2-yl)benzo[1,2-d;4,5-d′]bisthiazole)] (PBTHDDT, M_n = 19.94 kDa, PDI = 2.84) were reported elsewhere.[4i] Regioregular poly(3-hexylthiophene) (P3HT) (M_w = 35.40 kDa, PDI = 2.45) was purchased from Rieke Metals. The fullerenes, [6,6]-phenyl-C_{71}-butyric acid methyl ester ($PC_{71}BM$, >99.0%), [6,6]-phenyl-C_{61}-butyric acid methyl ester ($PC_{61}BM$, >99.5%), and indene–C_{60} bisadduct ($IC_{60}BA$, >99%) were purchased from Nano-C, American Dye Sources, Inc., and Luminescence Technology Corp., respectively. Anhydrous *ortho*-dichlorobenzene (ODCB), and 1,8-diiodooctane (DIO) were obtained from Sigma Aldrich. All commercial products were used without further purification.

Characterization of Energy Levels: CV was carried out on an EG&G Princeton Applied Research potentiostat/galvanostat (Model 273A), and the data were analyzed using a Model 270 electrochemical analysis system software. A three-electrode cell was used, with platinum wires as both counter and working electrodes, and Ag/Ag^+ (Ag in 0.1 M $AgNO_3$ solution, Bioanalytical System, Inc.) as a reference electrode. A thin film of each semiconductor was coated onto a platinum electrode from a concentrated solution in chloroform and dried in vacuum. Solution CV was performed with 10 mg of solute in a 0.1 M solution of $TBAPF_6$ in benzene/acetonitrile (11.3 mL/3.8 mL) under N_2. Using the ferrocenium/ferrocene (Fc^+/Fc) redox couple as an internal standard, the redox potential values were obtained in reference to a Ag/Ag^+ electrode. All solutions were purged with N_2 for 20 min before each experiment. Solid state *IE* and *EA* values were estimated from CV (relative to SCE) using the relationship of, $EA = eE_{red}^{onset} + 4.4$ eV and *IE* using the relationship $IE = eE_{ox}^{onset} + 4.4$ eV.[26]

UPS measurements were performed under ultrahigh vacuum conditions using the He(I) photon line (21.22 eV) from a He discharge lamp. The energy resolution of the measurement was 0.15 eV. A −5 V bias was applied to the sample to facilitate the observation of the slow electron cutoff. IPES measurements were conducted in the isochromat mode, detecting photons with an energy of ≈10 eV. For the measurements, the energy of the exciting electrons produced by a low energy electron gun was swept from ≈5 to 15 eV. Degradation of the sample was minimized by varying the position of the electron beam on the surface, so that no single spot was exposed for longer than 2 min. The overall IPES instrumental resolution is 450 meV, estimated from the width of a metal Fermi edge. The substrates prepared for UPS and IPES measurements consisted of ozone treated indium tin oxide (Thin Film Technology) covered by approximately 20 nm of PBTHDDT or each fullerene derivative. The *IE* and *EA* were derived by fitting the onset of the density of states by a linear slope and measuring the intersection of this fit with the background signal.

Device Fabrication and Characterization: ODCB solutions of 10 mg/mL PBTHDDT, 20 mg/mL P3HT, and 60 mg/mL fullerene ($PC_{71}BM$, $PC_{61}BM$, or $IC_{60}BA$) were prepared and stirred until complete dissolution. All solutions were passed through 0.45 μm filters before use. Blend solutions of PBTHDDT:fullerene and P3HT:fullerene were prepared by mixing respective solutions at desired weight ratio.

Solar cells were fabricated on ITO-coated glass substrates (10 Ω/, Shanghai B. Tree Tech, China). The substrates were cleaned sequentially with acetone, deionized water, isopropyl alcohol in an ultrasonic bath, and dried in a vacuum oven. A 40 nm PEDOT:PSS (Clevios P VP AI 4083) layer was spin-coated on top of the ITO and dried at 150 °C for 10 min under vacuum. The blend solution, which is either PBTHDDT:fullerene (containing 2.5 vol% DIO) or P3HT:fullerene blend, was spin-coated on top of PEDOT:PSS to make a BHJ active layer of ≈80 nm in the glovebox. The active layer was then dried in vacuum for 2 h (PBTHDDT:fullerene) or aged in a Petri dish for 30 min and annealed at 175 °C for 10 min (P3HT:fullerene). The substrates were then loaded in a thermal evaporator (BOC Edwards, model 306) to deposit a cathode composed of 1.0 nm LiF and 80 nm Al under high vacuum (8×10^{-7} Torr). Four solar cells, each with an active area of 9 mm^2, were fabricated per ITO substrate.

Current–voltage characteristics of the non-encapsulated solar cells were obtained using an HP4155A semiconductor parameter analyzer in ambient laboratory air. The 1 Sun illumination (AM1.5 at 100 mW/cm^2) was provided by a filtered Xe lamp and calibrated by using a Si diode calibrated at the National Renewable Energy Lab (NREL, USA). Incident photon-to-current efficiency (IPCE) was measured using a QEX10 solar cell quantum efficiency measurement system (PV Measurements, Inc.).

Characterization of Morphology: AFM imaging was performed on the same solar cell devices using a Dimension 3100 SPM (Veeco) instrument operating in tapping mode. Thin films of the active layers were obtained by scratching edges of the thin films, soaking with water, and peeling them off from the device substrates, and they were then supported on TEM grids (Electron Microscopy Sciences) for BF-TEM imaging. An FEI Tecnai G^2 F20 TEM at 200 kV was employed. Images were slightly defocused to enhance the phase contrast between the polymer and fullerene, and were acquired with a CCD camera and recorded with Gatan DigitalMicrograph software.

UV-Vis Absorption and PIA Spectra: UV-vis absorption spectra of neat polymer or fullerene films were recorded with a Perkin-Elmer model Lambda 900 UV/vis/near-IR spectrophotometer using glass substrate. UV–vis absorption spectra of blend films were recorded on the blend films spin-coated on top of PEDOT/ITO substrates, following the same processing conditions as the solar cells. PIA spectra were collected as previously described[27] using conventional lock-in detection methods[28] employing either a 455 nm or 630 nm LED excitation source modulated at 200 Hz. Measurements were performed in transmission mode on glass substrates in a Janis cryostat at 80 K. Spectroelectrochemical measurements were performed at room temperature on PBTHDDT films deposited on ITO substrates immersed in acetonitrile:tetrabutylammonium perchlorate solution with a silver reference electrode in a Cary UV-vis-NIR spectrophotometer.

Supporting Information

Supporting Information is available from the Wiley Online Library or from the author.

Acknowledgements

This work was based on research (excitonic solar cells) supported by the U.S. DOE, Basic Energy Sciences, Division of Materials Science, under Award No. DE-FG02-07ER46467. S.A.J. and A.K. also acknowledge the support by Solvay S.A. for the synthesis of the polymer and UPS/IPES experiments. C.W.S. acknowledges partial support through the U.S. NSF SEES fellowship program (analysis, GEO-1215753). S.O. acknowledges the German Academic Exchange Service (DAAD) for a postdoctoral fellowship. The authors gratefully acknowledge Dr. Michael A. White and Prof. Daniel R. Gamelin for their contributions to the spectroelectrochemical data in this work and Dr. Nishit Murari for useful discussions. Part of this work was conducted at the UW NanoTech User Facility, a member of the NSF National Nanotechnology Infrastructure Network (NNIN).

Received: June 1, 2012
Revised: September 9, 2012
Published online: October 16, 2012

[1] a) K. M. Coakley, M. D. McGehee, *Chem. Mater.* **2004**, *16*, 4533–4542; b) S. Gunes, H. Neugebauer, N. S. Sariciftci, *Chem. Rev.* **2007**, *107*, 1324–1338; c) B. C. Thompson, J. M. J. Fréchet, *Angew. Chem. Int. Ed.* **2008**, *47*, 58–77; d) G. Dennler, M. C. Scharber, C. J. Brabec, *Adv. Mater.* **2009**, *21*, 1323–1338; e) F. G. Brunetti, R. Kumar, F. Wudl, *J. Mater. Chem.* **2010**, *20*, 2934–2948; f) P.-L. T. Boudreault, A. Najari, M. Leclerc, *Chem. Mater.* **2010**, *23*, 456–469; g) G. Li, R. Zhu, Y. Yang, *Nat. Photonics* **2012**, *6*, 153–161.

[2] G. Yu, J. Gao, J. C. Hummelen, F. Wudl, A. J. Heeger, *Science* **1995**, *270*, 1789–1791.

[3] a) Y. Liang, Z. Xu, J. Xia, S. T. Tsai, Y. Wu, G. Li, C. Ray, L. Yu, *Adv. Mater.* **2010**, *22*, E135–E138; b) C. E. Small, S. Chen, J. Subbiah, C. M. Amb, S.-W. Tsang, T.-H. Lai, J. R. Reynolds, F. So, *Nat. Photonics* **2012**, *6*, 115–120; c) Z. He, C. Zhong, S. Su, M. Xu, H. Wu, Y. Cao, *Nat. Photonics* **2012**, *6*, 593–597.

[4] a) J. Peet, J. Y. Kim, N. E. Coates, W. L. Ma, D. Moses, A. J. Heeger, G. C. Bazan, *Nat. Mater.* **2007**, *6*, 497–500; b) J. K. Lee, W. L. Ma, C. J. Brabec, J. Yuen, J. S. Moon, J. Y. Kim, K. Lee, G. C. Bazan, A. J. Heeger, *J. Am. Chem. Soc.* **2008**, *130*, 3619–3623; c) E. Ahmed, F. S. Kim, H. Xin, S. A. Jenekhe, *Macromolecules* **2009**, *42*, 8615–8618; d) F. C. Krebs, *Sol. Energy Mater. Sol. Cells* **2009**, *93*, 394–412; e) G. Ren, P.-T. Wu, S. A. Jenekhe, *Chem. Mater.* **2010**, *22*, 2020–2026; f) G. Zhao, Y. He, Y. Li, *Adv. Mater.* **2010**, *22*, 4355–4358; g) G. Ren, P.-T. Wu, S. A. Jenekhe, *ACS Nano* **2011**, *5*, 376–384; h) P. Sonar, G.-M. Ng, T. T. Lin, A. Dodabalapur, Z.-K. Chen, *J. Mater. Chem.* **2010**, *20*, 3626–3636; i) E. Ahmed, S. Subramaniyan, F. S. Kim, H. Xin, S. A. Jenekhe, *Macromolecules* **2011**, *44*, 7207–7219; j) S. Subramaniyan, H. Xin, F. S. Kim, S. Shoaee, J. R. Durrant, S. A. Jenekhe, *Adv. Energy Mater.* **2011**, *1*, 854–860; k) H. Xin, S. Subramaniyan, T.-W. Kwon, S. Shoaee, J. R. Durrant, S. A. Jenekhe, *Chem. Mater.* **2012**, *24*, 1995–2001; l) G. Ren, E. Ahmed, S. A. Jenekhe, *J. Mater. Chem.* **2012**, DOI: 10.1039/C2JM33787H.

[5] a) G. Ren, E. Ahmed, S. A. Jenekhe, *Adv. Energy Mater.* **2011**, *1*, 946–953; b) P. E. Schwenn, K. Gui, A. M. Nardes, K. B. Krueger, K. H. Lee, K. Mutkins, H. Rubinstein-Dunlop, P. E. Shaw, N. Kopidakis, P. L. Burn, P. Meredith, *Adv. Energy Mater.* **2011**, *1*, 73–81; c) E. Ahmed, G. Ren, F. S. Kim, E. C. Hollenbeck, S. A. Jenekhe, *Chem. Mater.* **2011**, *23*, 4563–4577; d) P.-T. Wu, H. Xin, F. S. Kim, G. Ren, S. A. Jenekhe, *Macromolecules* **2009**, *42*, 8817–8826; e) P.-T. Wu, G. Ren, S. A. Jenekhe, *Macromolecules* **2010**, *43*, 3306–3313.

[6] J. Zaumseil, H. Sirringhaus, *Chem. Rev.* **2007**, *107*, 1296–1323.

[7] a) A. Babel, S. A. Jenekhe, *J. Am. Chem. Soc.* **2003**, *125*, 13656–13657; b) A. Babel, J. D. Wind, S. A. Jenekhe, *Adv. Funct. Mater.* **2004**, *14*, 891–898; c) T. B. Singh, P. Senkarabacak, N. S. Sariciftci, A. Tanda, C. Lackner, R. Hagelauer, G. Horowitz, *Appl. Phys. Lett.* **2006**, *89*, 033512–033513; d) H. Usta, A. Facchetti, T. J. Marks, *J. Am. Chem. Soc.* **2008**, *130*, 8580–8581; e) F. S. Kim, X. Guo, M. D. Watson, S. A. Jenekhe, *Adv. Mater.* **2010**, *22*, 478–482.

[8] a) Y. He, Y. Li, *Phys. Chem. Chem. Phys.* **2011**, *13*, 1970–1983; b) Y. He, H.-Y. Chen, J. Hou, Y. Li, *J. Am. Chem. Soc.* **2010**, *132*, 1377–1382; c) Z.-L. Guan, J. B. Kim, H. Wang, C. Jaye, D. A. Fischer, Y.-L. Loo, A. Kahn, *Org. Electron.* **2010**, *11*, 1779–1785.

[9] a) P. Boland, S. S. Sunkavalli, S. Chennuri, K. Foe, T. Abdel-Fattah, G. Namkoong, *Thin Solid Films* **2010**, *518*, 1728–1731; b) H. Xin, F. S. Kim, S. A. Jenekhe, *J. Am. Chem. Soc.* **2008**, *130*, 5424–5542.

[10] a) K. Vandewal, K. Tvingstedt, A. Gadisa, O. Inganas, J. V. Manca, *Nat. Mater.* **2009**, *8*, 904–909; b) C. J. Brabec, A. Cravino, D. Meissner, N. S. Sariciftci, T. Fromherz, M. T. Rispens, L. Sanchez, J. C. Hummelen, *Adv. Funct. Mater.* **2001**, *11*, 374–380.

[11] S. S. van Bavel, E. Sourty, G. de With, J. Loos, *Nano Lett.* **2009**, *9*, 507–513.

[12] N. S. Sariciftci, L. Smilowitz, A. J. Heeger, F. Wudl, *Science* **1992**, *258*, 1474–1476.

[13] A. Sperlich, M. Liedtke, J. Kern, H. Kraus, C. Deibel, S. Filippone, J. L. Delgado, N. Martín, V. Dyakonov, *Phys. Status Solidi. RRL* **2011**, *5*, 128–130.

[14] D. M. Guldi, M. Prato, *Acc. Chem. Res.* **2000**, *33*, 695–703.

[15] M. D. Heinemann, K. von Maydell, F. Zutz, J. Kolny-Olesiak, H. Borchert, I. Riedel, J. Parisi, *Adv. Funct. Mater.* **2009**, *19*, 3788–3795.

[16] K. M. Noone, S. Subramaniyan, Q. Zhang, G. Cao, S. A. Jenekhe, D. S. Ginger, *J. Phys. Chem. C* **2011**, *115*, 24403–24410.

[17] a) Y. He, G. Zhao, B. Peng, Y. Li, *Adv. Funct. Mater.* **2010**, *20*, 3383–3389; b) C. Deibel, D. Mack, J. Gorenflot, A. Schöll, S. Krause, F. Reinert, D. Rauh, V. Dyakonov, *Phys. Rev. B* **2010**, *81*, 085202.

[18] a) S.-S. Sun, N. S. Sariciftci, *Organic Photovoltaics: Mechanisms, Materials, and Devices*, CRC Press, Boca Raton, FL **2005**; b) X. Gong, M. Tong, F. G. Brunetti, J. Seo, Y. Sun, D. Moses, F. Wudl, A. J. Heeger, *Adv. Mater.* **2011**, *23*, 2272–2277; c) Y. He, C. Chen, E. Richard, L. Dou, Y. Wu, G. Li, Y. Yang, *J. Mater. Chem.* **2012**, *22*, 13391–13394.

[19] a) R. H. Crabtree, *Energy Production and Storage: Inorganic Chemical Strategies for a Warming World;*, John Wiley & Sons Ltd., Chichester, UK **2010**; b) J. H. Delcamp, A. Yella, M. K. Nazeeruddin, M. Grätzel, *Chem. Commun.* **2012**, *48*, 2295–2297.

[20] C. W. Schlenker, M. E. Thompson, *Top. Curr. Chem.* **2012**, *312*, 175–213.
[21] D. Veldman, S. C. J. Meskers, R. A. J. Janssen, *Adv. Funct. Mater.* **2009**, *19*, 1939–1948.
[22] S. Cook, R. Katoh, A. Furube, *J. Phys. Chem. C* **2009**, *113*, 2547–2552.
[23] J. J. Benson-Smith, H. Ohkita, S. Cook, J. R. Durrant, D. D. C. Bradley, J. Nelson, *Dalton Trans.* **2009**, 10000–10005.
[24] A. A. Bakulin, A. Rao, V. G. Pavelyev, P. H. M. van Loosdrecht, M. S. Pshenichnikov, D. Niedzialek, J. Cornil, D. Beljonne, R. H. Friend, *Science* **2012**, *335*, 1340–1344.
[25] a) D. C. Coffey, A. J. Ferguson, N. Kopidakis, G. Rumbles, *ACS Nano* **2010**, *4*, 5437–5445; b) Y. W. Soon, T. M. Clarke, W. Zhang, T. Agostinelli, J. Kirkpatrick, C. Dyer-Smith, I. McCulloch, J. Nelson, J. R. Durrant, *Chem. Sci.* **2011**, *2*, 1111–1120.
[26] a) A. P. Kulkarni, C. J. Tonzola, A. Babel, S. A. Jenekhe, *Chem. Mater.* **2004**, *16*, 4556–4573; b) E. Ahmed, T. Earmme, G. Ren, S. A. Jenekhe, *Chem. Mater.* **2010**, *22*, 5786–5796.
[27] K. M. Noone, N. C. Anderson, N. E. Horwitz, A. M. Munro, A. P. Kulkarni, D. S. Ginger, *ACS Nano* **2009**, *3*, 1345–1352.
[28] D. S. Ginger, N. C. Greenham, *Phys. Rev. B* **1999**, *59*, 10622–10629.